The relation between magnesium evaporation and laser absorption and weld penetration in pulsed laser welding of aluminum alloys: Experimental and numerical investigations

Malekshahi Beiranvand, Z., Malek Ghaini, F., Naffakh Moosavy, H., Sheikhi, M., Torkamany, M. J. & Moradi, M.

Original citation & hyperlink:
Malekshahi Beiranvand, Z, Malek Ghaini, F, Naffakh Moosavy, H, Sheikhi, M, Torkamany, MJ & Moradi, M 2020, 'The relation between magnesium evaporation and laser absorption and weld penetration in pulsed laser welding of aluminum alloys: Experimental and numerical investigations', Optics and Laser Technology, vol. 128, 106170.
https://dx.doi.org/10.1016/j.optlastec.2020.106170

DOI 10.1016/j.optlastec.2020.106170
ISSN 0030-3992

Publisher: Elsevier

The relation between magnesium evaporation and laser absorption and weld penetration in pulsed laser welding of aluminum alloys: experimental and numerical investigations

Z. Malekshahi Beiranvand[1], F. Malek Ghaini[*1], H. Naffakh Moosavy[1], M. Sheikhi[2], M. J. Torkamany[3], M. Moradi[4, 5]

1- Department of Materials Engineering, Tarbiat Modares University, 14115-143, Tehran, Iran.
2- Department of Materials Engineering, Bu-Ali Sina University, 65178-38695, Hamedan, Iran.
3- Iranian National Center for Laser Science and Technology (INLC), 14665-576, Tehran, Iran.
4- Department of Mechanical Engineering, Faculty of Engineering, Malayer University, Malayer, Iran.
5-Laser Materials Processing Research Center, Malayer University, Malayer, Iran.

Abstract

It is observed that in laser welding of aluminum alloys, magnesium can evaporate, and the weld penetration is dependent on Mg content of the alloy and Mg loss from the weld pool. In this research, it is proposed that the presence of Mg not in the base metal alloy, but rather the presence of Mg vapor in the plasma plume over the weld pool affects the laser absorption, and it is through this phenomenon that the weld profile and penetration is affected. Numerical simulation was performed to determine the relationship between the weld profile to estimate the effective laser absorption coefficient of four Al alloys and in parallel EPMA technique was used to determine the Mg losses of the weld metals. The combined analysis of the results showed that increasing the laser pulse energy (decreasing laser pulse frequency), Mg evaporation is increased, and that, in turn, increased the effective laser absorption coefficient. However, more laser power absorption does not necessarily mean more weld penetration. Laser absorption results in weld penetration, once the threshold Mg evaporation rate of 200 x10^{-6} g/cm^2 is passed.

Keywords: Pulsed laser welding, aluminum alloys, magnesium content, evaporation, penetration depth, effective absorption coefficient

1. Introduction

The use of high-strength Al alloys in the transportation industry is increasing, especially in the manufacturing of wide-body aircraft. As a result, research has accelerated on the metallurgical phenomena governing the process of joining metal parts made of Al alloys. In laser welding of Al alloys, the laser reflection resulting from the poor coupling between Al alloys and laser

[*]Corresponding author. Tel.: +98 9121276087; fax: +98 21 88005040; e-mail: fmalek@modares.ac.ir

beams, Mg evaporation, and solidification cracking are significant challenges [1]. The laser vapor pressure of Mg exceeds that of Al. So, Mg is easily evaporated during pulsed and continuous Nd: YAG laser welding of Al alloys in both conduction and keyhole modes. This results in variations in the composition, which in turn can alter the mechanical and metallurgical properties of the weld metal [2, 3, 4, 5]. Temperature and composition are among the factors affecting the rate of Mg evaporation [6, 7, 2, 8]. Malekshahi et al. [9] upgraded the Langmuir's equation to calculate the rate of Mg evaporation in the pulsed laser welding of Al-Mg alloys in conduction mode, taking into account effects of overlapping of weld spots [2, 9]. Previous studies have also demonstrated that the trace of Mg in the weld metal has a significant impact on increasing the penetration depth and encouraging the keyhole mode [10, 4]. Katayama demonstrated that Al alloys having a higher concentration of volatile elements, e.g., Mg in 5000 alloys, were more easily melted and required a lower threshold power density to achieve satisfactory coupling between laser beam and Al alloys [1]. Some explanations have been put forward regarding the effects of Mg on weld metal penetration. It was argued that the presence of a surface-active element, such as Mg, increased the surface tension and enhanced the Marangoni effects, and as a result, the tendency to form a keyhole increased [11]. In another research, it was proposed that Al alloys with higher Mg content, had lower thermal conductivity. Thus, the heat was concentrated at the center of the weld pool, thereby increasing the penetration depth [7]. Another important issue related to the role of Mg in the welding of Al alloys is the presence of oxide, a major impurity in Al alloys. It was proposed that When Mg content of Al alloys approximately exceeds 2 wt%, the molten MgO plays a significant role in increasing the penetration depth [12, 13] by increasing surface tension as well as boosting laser energy absorption. The concentration of volatile alloying elements is one of the factors affecting the effective absorption coefficient of laser energy during welding [1]. In laser processes, the absorption coefficient of laser beams by the metal surface plays an important role in heat input generated by laser welding [11, 14, and 15]. However, experiments have demonstrated that the absorption coefficient of the laser beam by Al alloys is relatively low [1, 11]. The weak coupling of laser energy in such alloys is due to the high density of free electrons in the solid, making aluminum one of the best reflectors of light [1].

The interaction between the laser beam and the powdered materials used in the selective laser sintering process (SLS) has been investigated based on the type of materials and laser. However,

the interaction between the laser beam and the powder particles cannot be extended directly to that between a solid metal and the laser [16]. In 1995, Beck et al. [17] determined the effects of plasma on the intensity of the beam in deep penetration CO_2 laser welding with the help of the paraxial wave equation demonstrating that the heat loss parameters in the plasma plumes depend on laser wavelength and the characteristics of the plasma plumes (plasma temperature and electron density) [17].

Employing an experimental approach coupled with numerical analysis, the present research intends to investigate the relationship between the Mg evaporation, the weld penetration, and the effective Laser absorption coefficient in pulsed laser welding of Al alloys.

2. Method

2.1.Experimental

Four sheets of Al alloys, having different Mg contents, i.e., 2024-T851, 6061-T4, 5454-O and 5083-H321, with dimensions of 10 cm × 10 cm and thickness of 2 mm were used. The chemical composition of the alloys, as presented in Table 1, was determined by optical emission spectroscopy.

Table 1- The Chemical Composition of Al Alloys (weight percent)

Aluminum alloy	Ti	Zn	Cr	Mg	Mn	Cu	Fe	Si
6061-T4	0.02	0.03	0.19	0.75	0.15	0.2	0.31	0.59
2024-T851	0.05	0.08	0.05	1.45	0.61	4.3	0.3	0.16
5454-O	0.01	Trace	0.1	3.04	0.79	0.07	0.3	0.1
5083-H321	0.01	Trace	0.06	4.3	0.72	0.01	0.15	0.15

For welding, a pulsed Nd: YAG laser machine, model IQL-10, with a maximum power of 400 W was used. This machine can produce square pulses with 0.2-20ms width and with the frequency of 1-1000 Hz having maximum energy of up to 40 J. If the output power of the laser does not exceed 400 W, any combination of these parameters can be used. A lens with a focal length of 75 mm was used to focus the laser beam. A CNC table with X, Y, and Z directions and with a precision of 0.05 mm was used to control the movement of the workpiece and the welding speed. To measure laser power, a power meter, model 5000W-LP, made by OPHIR, was used. In all samples under pulsed laser welding, argon was coaxially used as a shielding gas, having a 10 l/m

flow rate. The image of the laser equipment used to perform pulsed laser welding is shown in Fig. 1.

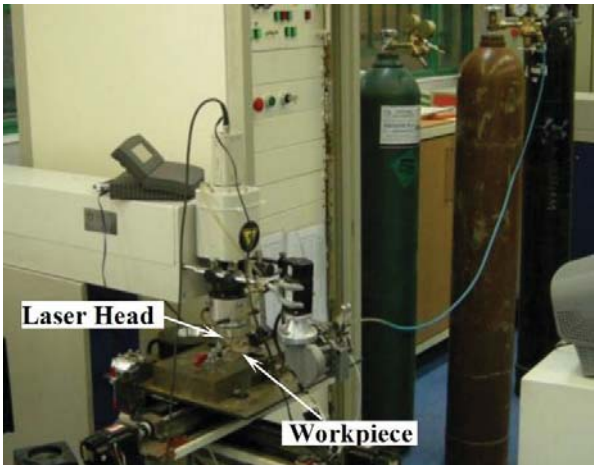

Figure.1. Pulsed laser welding set up used in the experiments.

Preliminary tests and experiments were conducted to increase the frequency at a constant welding speed. For this purpose, in the selection of the laser parameters, care was taken to ensure that all welds under investigation were in the conduction mode, having a fixed laser beam diameter (d_s), average power (P_M), and travel speed (V) set at 7×10^{-4} m, 200 W, and 5×10^{-3} m/s respectively. As shown in Table 2, the frequency, the duty cycle, and the overlapping factor increased from 15Hz to 40Hz, from 12% to 16%, from 55% to 82%, respectively. Pulse energy, however, reduced from 13.3 to 5 J. Therefore, the heat input applied to the workpiece (HI = P / V) was constant. The diagram in Fig. 2 illustrates the relationship between the pulse shape and the laser parameters. Accordingly, the duty cycle (DC) is equal to the accumulation of the duration of the laser pulse on time, t_P, divided by the total time (pulse on- and off-time), t_F. The pulse frequency is equal to 1 divided by t_F. The pulse energy (E_P) can be obtained from multiplying peak power, P_P, and pulse duration, t_P, and is equal to the pulse shape area. Pulse duration is the amount of time the laser pulse is set to the "on" mode. Therefore:

$$E_P = P_P \times t_P \quad (1)$$

Where average power, P_M, represents the average power of a laser source. The following relationship exists between average laser power, pulse energy, and frequency:

$$P_M = E_P \times f \quad (2)$$

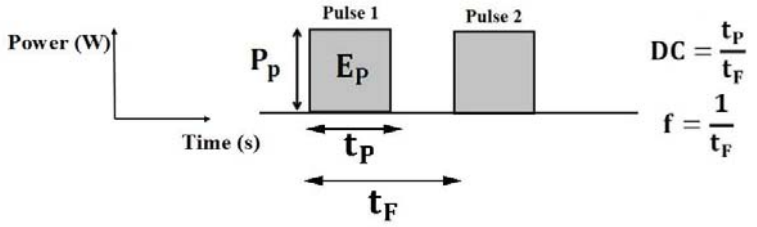

Figure. 2. Schematic of pulse shape and its relationship with laser parameters.

As the duty cycle increases, the duration of laser interaction with the material (t_{IN}), obtained from Equation 3, increases [18].

$$t_{IN} = \frac{d_s}{V} \times DC \tag{3}$$

Table 2 summarizes the parameters used to produce the experimental weld runs. After welding, the transverse cross-sections of the weld metals were studied by optical microscopy. To examine the extent to which Mg content varied in the investigations, analysis of the weld metal was performed by an Electron Probe Microanalyzer (EPMA), SX100 model. The chemical investigations were performed on an area equal to 5×10^{-6} m $\times$ 5×10^{-6} m. From each weld sample, three locations were studied; the average content of their Mg was reported.

Table 2- Pulse laser welding parameters used to create welding lines

Test run identification number	**1**	**2**	**3**	**4**
Laser pulse frequency (Hz)	15	20	25	40
Pulse Energy (J)	13.3	10	8	5
Pulse duration (s)	0.007	0.006	0.005	0.004
Peak power (K W)	1.9	1.6	1.6	1.25
Duty cycle (%)	10.5	12	12.5	16
Overlap factor (%)	55	65	72	82
Travel speed (m/s)	0.005	0.005	0.005	0.005
Average power (W)	200	200	200	200
The Heat input (J/mm)	40	40	40	40
Peak power density(kW/mm^2)	1.23	1.04	1.04	0.81

2.2.Simulation

A finite-element model was developed for pulsed laser welding, where the effects of the process parameters on the temperature of the weld pool and accordingly weld profiles were studied to estimate the effective absorption coefficient of the laser beam in various conditions.

2.2.1. Governing Equations and the Boundary Conditions

A three-dimensional symmetric model was simulated. The most advantage of axisymmetric modeling is the reduction in the number of elements, and in turn, the reduction in the calculation time. To simplify the modeling, the following assumptions were considered:

1. The model was in a homogenous form.
2. The heat transfer from the melt pool was ignored.
3. Some material properties were considered temperature-dependent.
4. Melt flow was ignored in the weld pool.

The overall analysis of the laser welding process with the help of the finite-element model is shown in Fig. 3. The analysis conducted in this research was thermal, aiming to obtain the element temperature in different nodes and times. Mesh area had 90288 elements of the type C3D8T. A smaller mesh size (about 8 μm) was used at the center of the weld pool region, while a larger mesh was used in the outer regions of the weld pool. A mesh-size independency test was conducted to determine the appropriate mesh size.

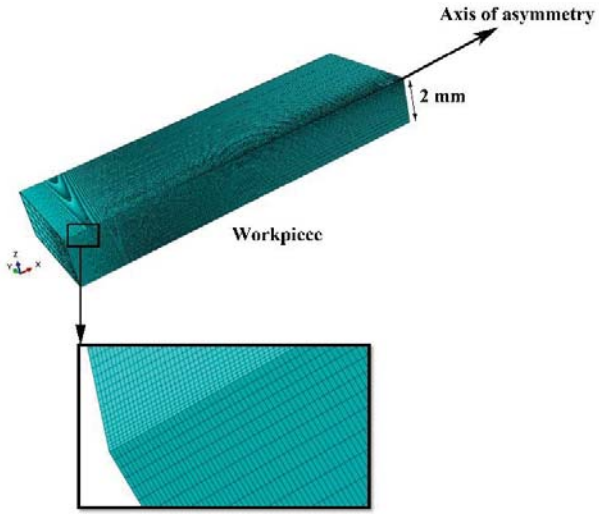

Figure. 3. Mesh details of finite-element model concerning pulsed laser welding

The governing equation of heat transfer was as follows [19]:

$$\left[\frac{\partial^2 T}{\partial x^2}\right] + \left[\frac{\partial^2 T}{\partial y^2}\right] + \left[\frac{\partial^2 T}{\partial z^2}\right] = \frac{\rho c_p}{k}\frac{\partial T}{\partial t} \quad (4)$$

In which C_p, k, ρ, T, and t are heat capacity, coefficient of thermal conductivity, density, temperature, and time respectively. The initial temperature of the workpiece was set to be the room temperature, i.e., 25°C. Apart from the top surface, in all external surfaces, heat transfer was considered convective and radiative in nature. In the upper surface, radiative and forced convective heat transfer was considered. Also, half the weld metal region was modeled. Fig. 4 illustrates the ideal instance where the modeling of a laser beam, as a heat source having adequate boundary conditions, was performed based on the axisymmetric model under investigation.

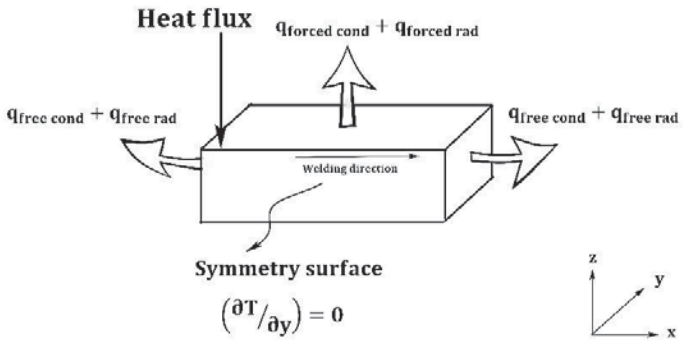

Figure. 4. Representation of surface heat flux and boundary conditions used for doing modeling numerically in the process of laser welding

2.2.2. Heat source model

To simulate laser radiation, heat flux was applied over the sample surface. Abaqus software could help (to) solve the problem. With the help of the Fortran programming language, the heat flux was further entered into the finite-element software using of the DFLUX subroutine, where the equation related to two-dimensional heat flux together with the distribution proposed by Goldack was used depending on the location and time of welding in conduction mode. The final equation is as follows [20]:

$$q = \frac{6P\eta_v\sqrt{3}}{a_1 a_2\ \pi\sqrt{\pi}} e^{\left[\left(\frac{-3}{a_1^2 + a_2^2}\right) * [y^2 + [x - x_0 - vt]^2]\right]} \quad (5)$$

In this equation, x_0 is the distance of the pulse overlapping; v is the speed of laser welding; x and y are the laser location; t is the time of welding; a_1 and a_2 are the surface dimensions of the weld pool ($a_1 = a_2 = 0.35$ mm); p is the average power of laser, and η_v is the effective laser absorption coefficient. The effective absorption coefficient for each alloy was separately estimated in each welding condition. For this purpose, the trial and error method was employed, in which various values of the effective absorption coefficient was applied to the input power until the geometrical dimensions of the simulated weld pool well fitted into the actual weld pool [21].

Table 3 indicates the factors involved in the computation mentioned above, within which specific heat, density, thermal conductivity, and elastic modulus were considered temperature-dependent [22]. For example, the temperature-dependent properties of the alloy 2024 are presented in Table 4. Furthermore, the emission coefficient, the Poisson's ratio, and the Stefan–Boltzmann constant were considered to be 0.022, 0.33, and 5.67 $\times 10^{-8} {}^{j}/_{sk^4m^2}$, respectively, according to the references [21, 23].

Table 3- The properties of Al alloys used in simulation of pulsed laser welding [5, 12].

Properties	2024 alloy	6061 alloy	5083 alloy	5454 alloy
Heat transfer coefficient on the top surface (W/m^2K)	20	20	20	20
Heat transfer coefficient on other surfaces (W/m^2K)	5	5	5	5
Thermal conductivity at 25 ^{0C} (W /m K)	151	154	117	134
The Specified heat capacity of solid (J/kg K)	875	896	924	900
The Specified heat capacity of liquid (J/kg K)	1273	1230	1261	1340
The Density of solid (kg/m^3)	2780	2700	2670	2070
The Density of liquid (kg/m^3)	2375	2240	2550	2010
Solidus temperature K (^0C)	775 (502)	855 (582)	848 (575)	875 (602)
Liquidus temperature K (^0C)	911 (638)	925 (652)	911 (638)	919 (646)
Modulus of elasticity at 298 K (25 ^0C)(N/m^2)	73.1×10^{-3}	68.9×10^{-3}	72×10^{-3}	69.6×10^{-3}
Thermal expansion at 298 K (25 ^0C) (1/K)	22.9×10^{-6}	22×10^{-6}	24×10^{-6}	23.7×10^{-6}

Table 4-Temperature-dependent properties of 2024 alloy [22]

Property	Conductivity	Density (10-9)	Young	Specific heat	Expansion

Temperature	(W /m K)	(kg/m^3)	modulus (N/m^2)	(J/kg K)	coefficient (10^{-5})
25	175	2785	72.4×10^{-3}	850	2.21
100	185	2770	66.5×10^{-3}	900	٢,٣
200	193	2750	63.5×10^{-3}	950	٢,٤
300	193	2730	60.4×10^{-3}	970	٢,٥١١٩
400	190	2707	56.1×10^{-3}	1000	٢,٥٥٩
500	188	2.683	50×10^{-3}	١٠٨٠	٢,٦٦٣٧
538	188	2.674		١١٠٠	
632	85.5	2.5		١١٤٠	
700	85	2.48		١١٤٠	
800	84	2.452		١١٤٠	

3. Results and Discussion

3.1.Simulation Results

3.1.1. Calculation of weld pool temperature

Simulation of the process of pulsed laser welding could help to estimate the temperature of the weld pool. Fig. 5 represents the thermal cycles of laser-welded 2024 Al alloy. As shown in Fig.5, the results of simulation showed that temperature decreased at the center of the weld pool with increasing the frequency since the pulse energy reduced when the frequency increased at constant average power, as shown by the experimental parameters presented in Table 2. Due to variations in the temperature of the molten pool during laser radiation, an average temperature (Ta) was used to simplify the measurement. The average temperature was estimated using the following equation:

$$T_a = \frac{\int_{t_s}^{t_f} T(t)dt}{t_f - t_s} \quad (6)$$

In this equation, t_s is the time when the melt starts to form, and t_f is the time when the solidification is completed.

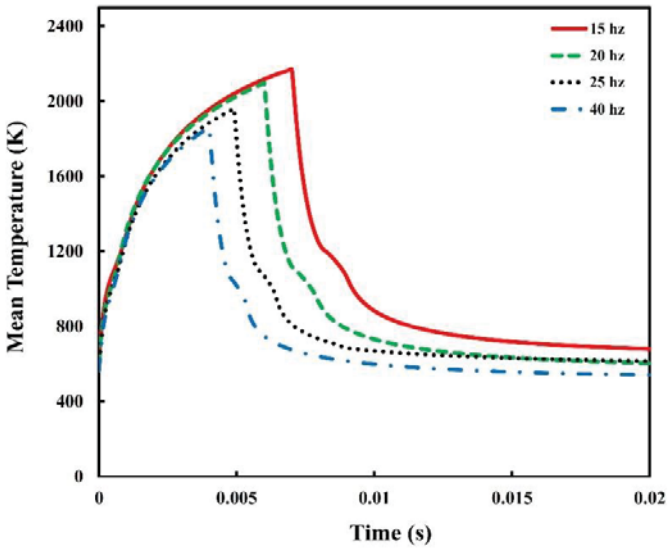

Figure. 5. The thermal history of the center of weld metal calculated for 5454 alloy in the fifth pulse at various frequencies of the pulse laser.

3.1.2. Estimation of the effective laser absorption coefficient by the workpiece

To estimate the effective absorption coefficient for various welding conditions, the similarity of the dimensions of the weld pool with that of the experimental results was taken into consideration. Fig. 6 shows the variations in the effective absorption coefficient with increasing frequency for each alloy. It can be observed that in each alloy, the effective absorption coefficient decreased with increasing the frequency. With increasing frequency, alloys with a higher Mg content displayed not only higher effective absorption coefficients but also a steeper change in the effective absorption coefficient.

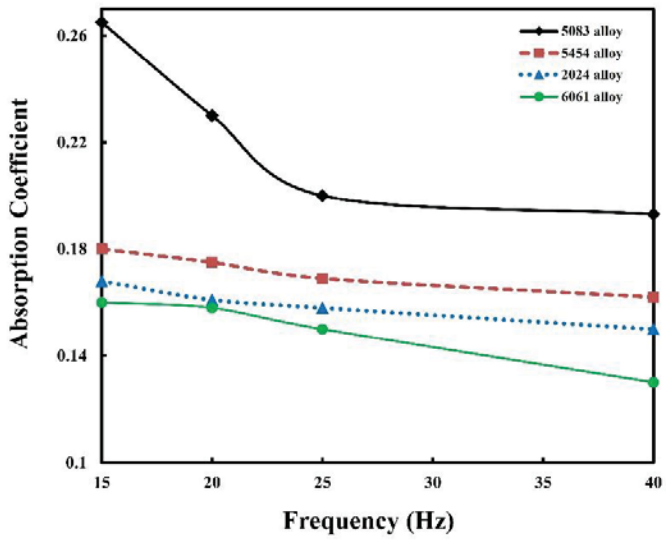

Figure. 6. Variations of effective absorption coefficient with increasing frequency obtained from the simulation of pulse laser welding for each Al alloy

3.2.The Validation of Simulation Results

The simulation process was validated for the 5454 alloy. To do so, a comparison was made between the dimensions of the actual weld pool and those obtained from the numerical results (Fig. 7).

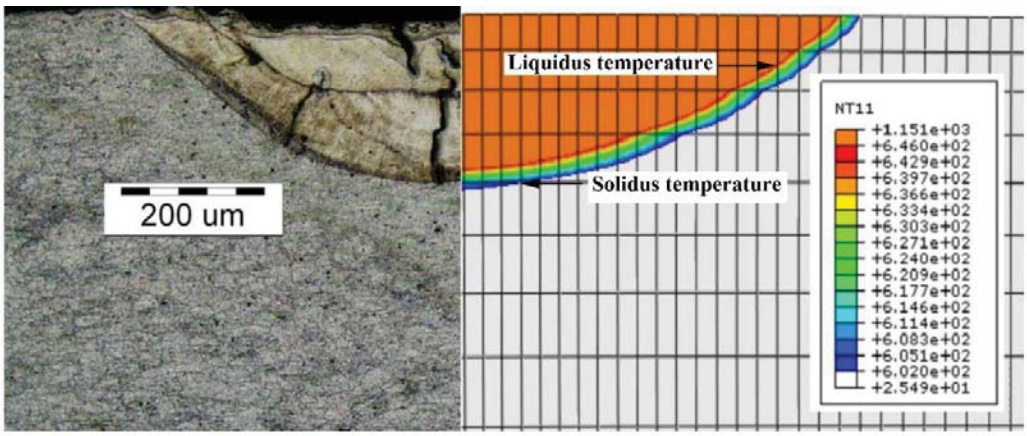

Figure. 7. Comparison of dimensions of actual weld pool with those obtained from 5454 alloy simulated at a frequency of 20 Hz. Temperatures higher than Liquidus (646 ^{0}C) are displayed in orange, and temperatures below Solidus (602 ^{0}C) are shown in white.

Furthermore, the real primary dendrite arm spacing (PDAS) derived from a scanning electron microscope (SEM) of the weld pool for the 5454 and 2024 Al alloys was compared with what was obtained from the simulation. To validate the predictions made based on the thermal model, including thermal gradient (∂T / ∂x) and cooling rate (∂T / ∂t), a relation was established in which primary dendrite arm spacing was related to thermal gradient and cooling rate as follows [24]:

$$\lambda_1 = 4.3\left(\frac{D\Gamma\Delta T_0}{k}\right) \times \left(\frac{\partial T}{\partial x}\right)^{-0.25} \times \left(\frac{\partial T}{\partial t}\right)^{-0.25} = C \times \left(\frac{\partial T}{\partial x}\right)^{-0.25} \times \left(\frac{\partial T}{\partial t}\right)^{-0.25} \quad (7)$$

Where D, Γ, ΔT_0, and k are diffusivity of solute in the liquid phase, Gibbs-Thomson coefficient, range of solidification, and equilibrium partition coefficient, respectively. C constant for Al-Mg alloys is as follows [24]:

$$\mathrm{C} = 0.0018\mathrm{m}^{0.75}\mathrm{k}^{0.5}\mathrm{s}^{-0.25}$$

And for Al-Cu alloys, C constant is [25]:

$$\mathrm{C} = 0.0007\mathrm{m}^{0.75}\mathrm{k}^{0.5}\mathrm{s}^{-0.25}$$

For 5454 alloy, the primary dendrite arm spacing was measured at a certain depth below the weld surface at a frequency of 20Hz. Then, the primary dendrite arm spacing was calculated using the values of (∂T / ∂x) and (∂T / ∂t) obtained at the same depth of the weld pool, and the results of the experimental measurements and the numerical calculations were compared. The SEM images of the welded sample of 5454 alloy, at a frequency of 20 Hz (Fig. 8), demonstrated that the primary dendrite arm spacing was 8×10^{-6} m. On the other hand, the predicted dendritic arm spacing concerning ∂T / ∂t (12×10^3 K / s) and ∂T / ∂x (3×10^5 K / m) was equal to 7×10^{-6} m, validating the accuracy of the simulation results. For 2024 alloy, the measured value of the primary dendrite arm spacing obtained from SEM images at a frequency 15 Hz was 2.7×10^{-6}m, while its value calculated based on the simulation results was 2.1×10^{-6}m.

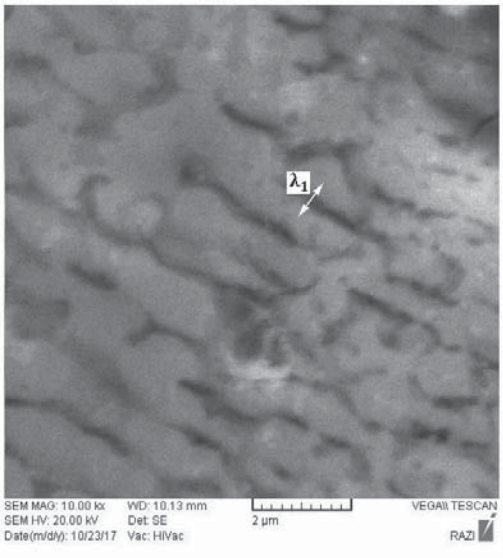

Figure. 8. SEM image of the cross-section of 5454 alloy weld metal at a frequency of 20 Hz indicating the primary dendrite arm spacing

3.3.Experimental Results

Fig. 9 shows the weld cross-sections of the 5083, 5454, 2024, and 6061 Al alloys, containing 4.5, 3.04, 1.45, and 0.75 Wt pct Mg, respectively. The given images were created at the 15Hz, 20Hz, 25Hz, and 40Hz pulse frequencies, respectively. It can be seen that penetration depth reduced when the pulse frequency increased, thereby lowering the weld metal volume. Also, the alloys with higher Mg content, especially 5083 alloy, suffered from this reduction more.

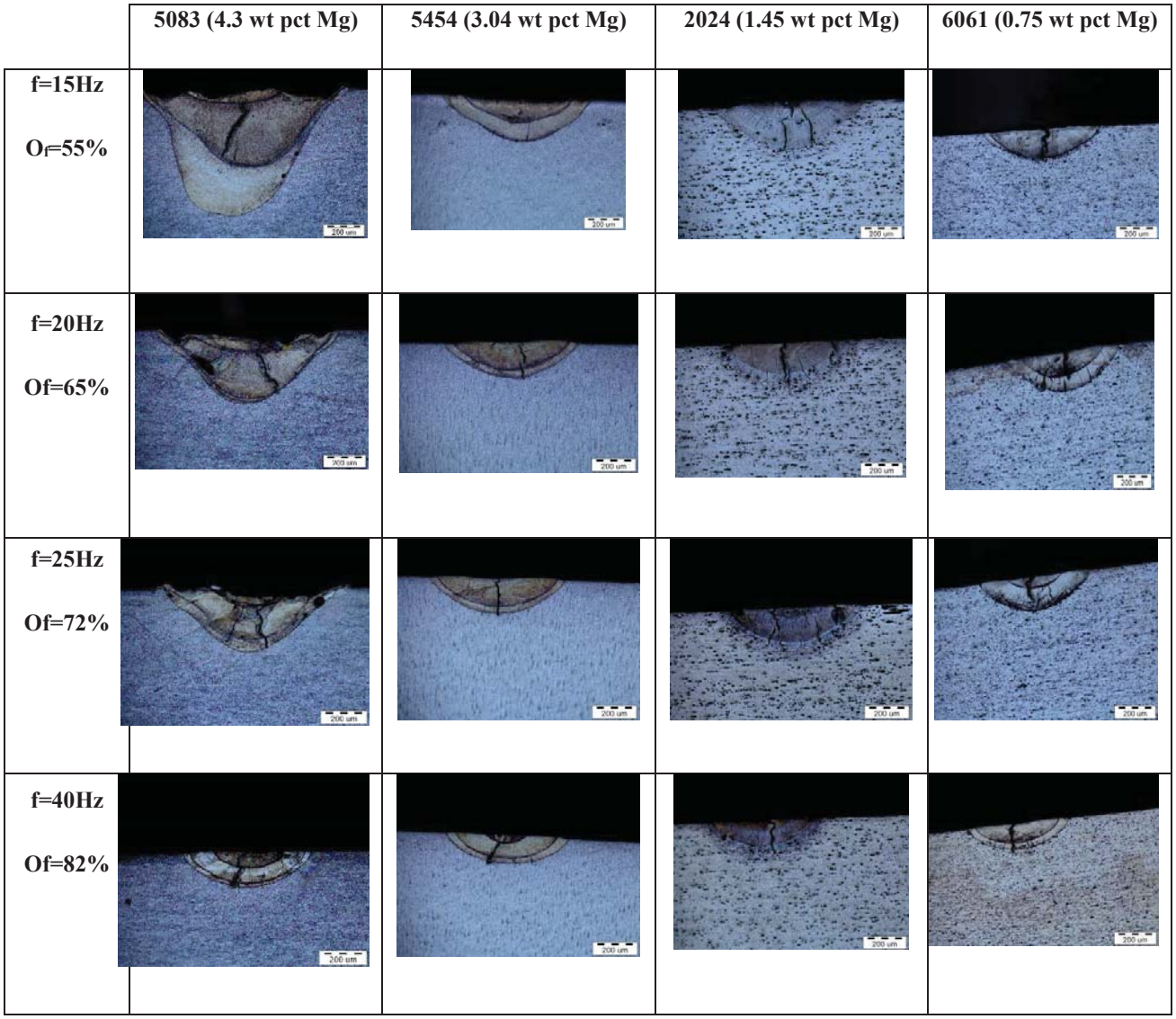

Figure. 9. Optical images for cross-sections of weld metals of Al alloys tested during experiments with a constant average power of 200 W and a constant speed of 5 mm/s while increasing frequency and overlapping factors.

Fig. 10a and 10b represent the variations observed in the penetration depth of various alloys as a result of increasing frequency and the changes found in the penetration depth due to the different Mg content at various pulse frequencies.

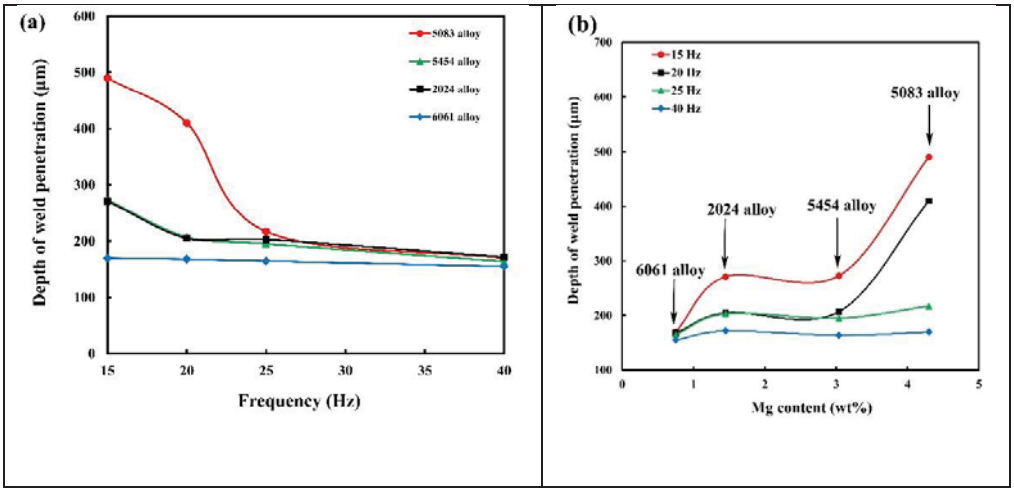

Figure. 10. a) Variations in penetration depth when increasing frequency of Al alloys using various amounts of Mg; b) variations in penetration depth by changing Mg content of base metal under conditions of constant frequency

Fig. 10a shows that in all alloys, increasing frequency reduced the penetration depth. The 5083 alloy, containing the highest Mg content, had the most upper penetration depth at the frequency of 15 Hz. As seen in the metallographic images, although the parametric conditions of the welding were set to the conduction mode, the keyhole mode was created in the 5083 alloys at a frequency of 15 Hz. When the frequency increased, this keyhole mode was transformed into the conduction mode, resulting in the reduced penetration depth. In the case of the 5454 alloy (3.04% Mg), the penetration depth decreased with an increase in the frequency. However, this reduction in the penetration depth was less than that in the 5083 alloy (4.5% Mg). The variations observed in the penetration depth in the 2024 alloy (1.45% Mg) while increasing frequency was approximately similar to those found in the 5454 alloy. However, in the case of 6061 alloy (0.75% Mg), having a much lower Mg content than the other three alloys, there were no variations in the penetration depth when the frequency increased. Fig. 10b shows that in constant welding conditions (constant frequency), the Al alloy with a higher Mg content had greater penetration depth. In fact, at the same welding frequency, increasing the percentage of Mg content in the alloy increased the penetration depth of the weld.

The reduction in the penetration depth with increasing the frequency can be justified if the laser parameters and simulation results are further studied. For this purpose, the cumulative pulse factor (F) and the interaction time between the pulse laser and the surface of the workpiece (t_{IN}) were calculated. Because the energy pumped to an area originates from not only a single pulse

but also overlapping pulses on the same spot, one can expect that neither peak power density nor heat input can fully explain the behavior of the laser pulsed welds. Thus, a cumulative pulse factor was introduced to take into account the role of a set of pulses hitting the spot [26]. The results are presented in Table 5. It should be noted that the temperatures mentioned in Table 5 are related to the 2024 alloy, obtained from the simulation results.

Table 5. Interaction of pulse laser welding parameters affecting penetration depth.

Test run identification number	f(Hz)	F	$E_p \times O_f$	t_{IN}(s)	T (K)
1	15	1.55	731.5	0.147	۱۸۸۰
2	20	1.9	650	0.168	۱۷۵۰
3	25	2.25	576	0.175	۱۶۶۰
4	40	3.3	410	0.224	۱۵۹۰

When the frequency increased, two factors, i.e., the reduced pulse energy competed against the increased pulse overlapping factor and the increased interaction time. As shown in Table 5, as the frequency increased, the multiplication of the pulse energy by the pulse overlapping factor decreased. Therefore, increasing the frequencies can be expected to decrease the penetration depth. The experimental results are shown in Fig. 9 support this argument.

The effect that is proposed regarding Mg is that at the beginning of laser radiation on aluminum, a large part of the laser beam is reflected. Al is highly reflective due to its low resistance to the free electron motion. However, in the Al-Mg alloys, such as 5083, due to the much lower evaporation temperature of Mg compared to Al, some Mg evaporates from the metal surface. The presence of the Mg in the plasma plume enhances the coupling between the workpiece and the laser beam (See Fig. 11).

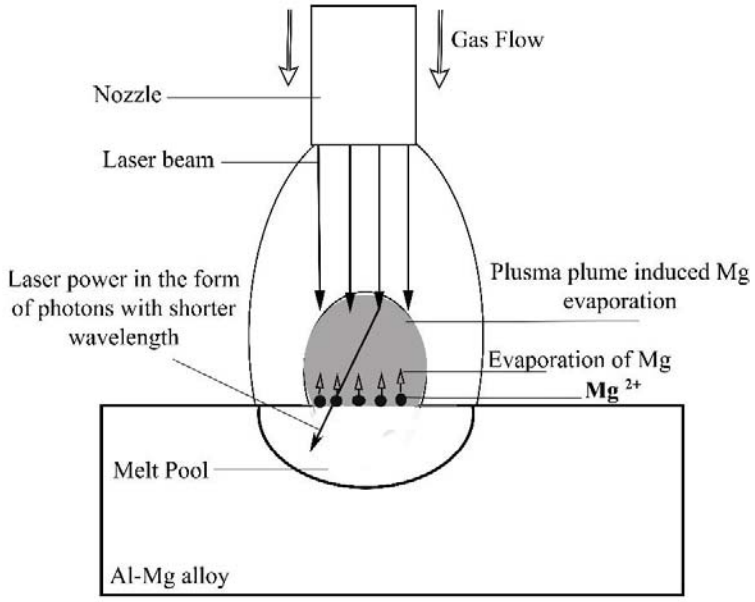

Figure 11. The schematic of the effect of Mg evaporation on increasing effective laser absorption. Plasma plume induced Mg evaporation reradiates laser power in all directions in the form of a photon with shorter wavelengths, resulting in the laser beam easier to be absorbed by the workpiece.

As already stated, when the frequency increased, both pulse energy and temperature at the center of the weld pool decreased. Consequently, even if Mg content of the base metal was high, the intensity of Mg evaporation and the formation of plasma plume filled Mg vapor is reduced, and consequently the effective laser absorption the penetration depth is decreased.

At the frequency of 15 Hz, in the 5454 alloy, although the temperature at the center of the weld pool was similar to that in the 5083 alloy, the penetration depth was lower, due to the lower Mg content of the base metal. As a result, less Mg was evaporated (less Mg loss), and less laser energy was absorbed. This was in agreement with the simulation results. The simulation results (Fig. 6) demonstrated that the alloys with a higher Mg content, such as 5083, had a higher effective absorption coefficient. Moreover, increasing the frequency decreased the effective absorption coefficient of the weld pool in all alloys.

Fig. 12 shows the amount of Mg evaporation per unit area. The results indicate that for 5083 and 5454 alloys, the decrease in Mg evaporation intensity is more noticeable when the frequency is increased.

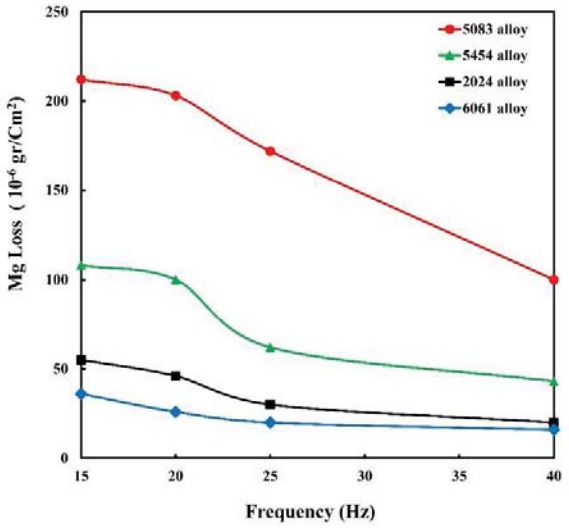

Figure. 12- Results of EPMA analysis concerning Mg evaporation per unit surface area of weld metal as a function of frequency in pulsed laser welding of Al alloys.

Fig. 13 shows the relation between the calculated Mg loss from the weld pool in terms of g/cm^2 and the weld penetration in the Al alloys with different Mg contents at different laser pulse frequencies. The data shows that the weld penetration is a function of both the Mg content of the aluminum alloy and the Mg evaporation from the weld pool surface in the process of pulsed laser welding. It seems that the same weld penetration, for example, 0.2 mm, may be obtained with significantly different levels of Mg evaporation. However, further analysis of the data revealed that Mg evaporation could be the prime factor but in a more complex set of effects.

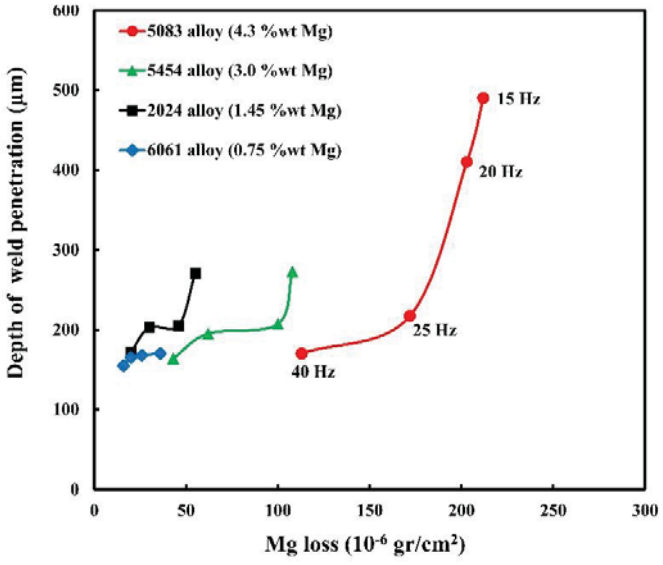

Figure. 13. The relation between Mg evaporation and depth of pulsed laser weld penetration for different Al alloy welds made at different laser pulse frequencies.

In figure 14, instead of weld penetration, the effective laser absorption is examined as a function of Mg evaporation. Now it can be seen that there is a clear correlation between the Mg evaporation per unit weld surface area and effective laser power absorption for all four aluminum alloys made at all four pulse frequencies examined. On the other hand, it has to be noted that higher laser absorption does not necessarily mean higher weld penetration, since in some circumstances, the laser absorption may be in such a way that the base material is melted but not penetrated, i.e., the laser is in a rather fully conduction mode.

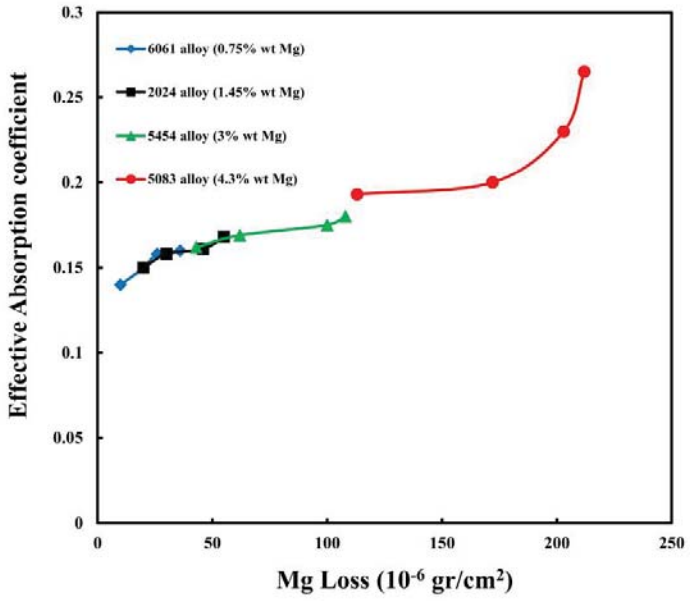

Figure. 14. The relation between Mg evaporation and effective laser power absorption for different Al alloy welds made at different laser pulse frequencies.

The data indicate that although Mg evaporation increases laser absorption, there is a threshold regarding the effectiveness of Mg evaporation on increasing the weld penetration. When Mg evaporation is low (until below the threshold value of effective Mg evaporation), aluminum alloys behave similarly regarding weld penetration, although Mg containing alloys due to the presence of Mg vapor absorbs more laser power. Please see figure 13 and compare penetrations of welds made at 40 Hz laser pulse frequency (lower laser pulse energies); the higher Mg content alloys have the same weld penetration, although we know from figure 14 that more power is absorbed. However, for welds made at low laser pulse frequencies of 15Hz i.e., high pulse energies, the situation is different. At high pulse energy, once a threshold Mg evaporation is

passed, not only effective laser power absorption coefficient is increased, but also the plasma plume formed above the weld pool changes its behavior, and a keyhole is formed and weld penetration in an Mg containing alloy is increased significantly.

Conclusion

The effect of the presence of Magnesium in Aluminum alloys, laser pulse frequency (pulse energy) on weld penetration, Mg loss of the weld metal, and effective laser power absorption was studied by experimental and numerical means. It is established that the changes in weld penetration, laser power absorption, and weld profile is not directly due to Mg in the alloy by itself. It is the Mg evaporation that affects the whole process. The effective laser power absorption has a positive correlation with Mg evaporation and it can increase from 0.14 to 0.265 as the Mg evaporation was increased by increasing the laser pulse energy from 5 J to 13.3 J (decreasing the pulse frequency from 40Hz to 15Hz). However, more laser power absorption does not necessarily mean more weld penetration. At low Mg evaporation rates, aluminum alloys in terms of weld penetration behave similar to each other irrespective of Mg content as the weld is in a full conduction mode, i.e., more laser power absorption results in the spread of the heat source. The Mg evaporation rate once passing a threshold of about 200 $x10^{-6}$ g/cm^2, the formation of a keyhole is facilitated, and the weld penetration and laser absorption both increase significantly and alloys with different levels of Mg behave differently.

References

[1] Pastor M, Zhao H, Martukanitz RP, Debroy T. Porosity, underfill and magnesium loss during continuous wave Nd: YAG laser welding of thin plates of Aluminum alloys 5182 and 5754. Welding Research supplement; 1999; 207-216.

[2] Zhao H, White DR, Debroy T. Current issues and problems in laser welding of automotive Aluminum alloys. International Materials Reviews; 1999; 44: 238-266.

[3] Jandaghi M, Parvin P, Torkamany M J, Sabbaghzadeh J. Alloying element losses in pulsed Nd: YAG laser welding of stainless steel 316. J. Phys. D: Appl. Phys; 2008; 41: 235503.

[4] Creslak M J, Fuerschbach PW. On the weldability, composition, and hardness of pulsed and continuous Nd: YAG laser welds in Aluminum alloy 6061, 5456 and 5086. Metallurgical Transactions B; 1988; 19B: 319-329.

[5] Bag S, De A. Computational modeling of conduction mode laser welding process. In: Xiaodong Na, stone (Ed.). Laser welding, Intech; 2010, p.133-160.

[6] Miller Carl B: Laser welding Article, U.S. Laser corporation; 2016.

[7] Moon DW, Metzbower EA. Laser Beam Welding of Aluminum Alloy 5456. Welding research supplement; 1983; 53-58.

[8] Weston JP, Jones IA, Wallach ER. Laser welding of Aluminum alloys using different laser sources. 6th International Conference on Welding and Melting by Electron and Laser Beams;1998.

[9] Malekshahi Beiranvand Z, Malek Ghaeini F, Naffakh Moosavy H, Sheikhi M, Torkamany MJ. Magnesium Loss in Nd: YAG Pulsed Laser Welding of Aluminum Alloys. Metallurgical and Materials Transactions B; 2018; 49: 2896–2905.

[10] Yamaoka H, Yuki M, Tsuchiya K. Study of prevention of solidification cracking in Al-Mg-Si alloy laser welds CO2 laser welding. Quarterly Journal of the Japan welding society; 2000; 18: 422-430.

[11] Pierron N, Sallamand P, Matter S. Study of Magnesium and Aluminum alloys absorption coefficient during Nd: YAG laser interaction. Applied surface science; 2007; 253: 3208-3214.

[12] Zhang R, Fan D, Katayama S. Electron beam welding with activating flux, Electron beam. Transactions of JWRJ; 2006; 32.

[13] Qin G, Wang G, Zou Z. Effect of activating flux on the CO_2 laser welding process of 6013 Al alloy. Trans Nonferrous Met Soc China; 2007; I7:4x6-390.

[14] Achebo JI. A parametric analysis of the CO_2 laser heat absorption profile of 5083 Aluminum alloy. International journal of engineering science and technology; 2010; 2: 2029-2033.

[15] Pierron N, Sallamand P, Jouvard JM, Cicala E. Determination of an empirical law of Aluminum and magnesium alloys absorption coefficient during Nd: YAG laser interaction. Journal of Physics D: applied physics; 2007; 40: 2096-2101.

[16] Kurth JP, Wang X, Laoui T, Froyen L. Laser and materials in selective laser sintering. Assembly Automation; 23; 4: 357-371.

[17] Hosseini Motlagh NS, Parvin P, Jandaghi M, Torkamany MJ. The influence of different volume ratios of He and Ar in shielding gas mixture on the power waste parameters for Nd: YAG and CO2 laser welding. Optics and Laser Technology; 2013; 54: 191-198.

[18] Suder W. Use of fundamental laser material interaction parameters in laser welding. Journal of laser applications; 2012; 24.

[19] Zain-ul-abdein M, Nelias D, Jullien J, Deloison D. Experimental investigation and finite element simulation of laser beam welding induced residual stresses and distortions in thin sheets of AA 6056-T4. Materials Science and Engineering; 2010; 527: 3025-3039.

[20] Rahman chukhan J, Vasudevan M, Muthukumaran S, Ravi Kumar R. Simulation of laser butt welding of AISI 316L stainless steel sheet using various heat sources and experimental validation. Journal of Materials Processing Technology; 2015; 219: 48–59.

[21] Bergman T, Lavine A, Incropera F, Witt D De. Fundamentals of Heat and Mass Transfer. 5th ed. New York: Wiley; 2002; Chapter 7: pp. 268–324.

[22] Du J, Wei Z. Numerical investigation of thermocapillary-induced deposited shape in fused-coating additive manufacturing process of aluminum alloy. J Phys Commun; 2018; 2: 115013.

[23] Zhao N, Yang Y, Han M, Luo X, Feng G, Zhang R. Finite element analysis of pressure on 2024 Aluminum alloy created during restricting expansion-deformation heat-treatment. Trans Nonferrous Met Soc China; 2012; 22: 2226-2232.

[24] Kurz W, Fisher DJ. Fundamental of solidification. 3th ed. Trans Tech Publications: Switzerland – Germany - UK – USA; 1992: pp.133-300.

[25] Michaud EJ, Kerr HW, Weckman DC: Trend in welding research. proceeding of the 4th international conference; 1995; pp. 153-158.

[26] Malek Ghaini F, Torkamany MJ, Sabbaghzade J. Weld metal microstructure characteristics in pulsed Nd:YAG laser welding. Scripta Materialia; 2007; 56: 955-958.